TRANSPORT PROBLEMS 2019 Volume 14 Issue 1
PROBLEMY TRANSPORTU DOI: 10.21307/tp.2019.14.1.3

Keywords: Matlab; simulation; car; human; speed bump

Tomasz HANISZEWSKI*, Agata MICHTA
Silesian University of Technology, Faculty of Transport
Krasinski 8, 40-019 Katowice, Poland
**Corresponding author*. E-mail: tomasz.haniszewski@polsl.pl

PRELIMINARY STUDIES OF VERTICAL ACCELERATION OF A PASSENGER CAR PASSING THROUGH THE SPEED BUMP FOR VARIOUS DRIVING SPEEDS

Summary. The article proposes a phenomenological model of a passenger car. The model includes the biomechanical model of human bodies in the sitting position of Muksian and Nash acting as passengers, while the driver's weight has been reduced to the concentrated weight of the loading seat. The research carried out in this study consisted of passing the vehicle through a transverse obstacle along the so-called speed bump. Vehicle passes through the threshold at three different speeds: 10km/h, 20km/h, and 30km/h. The purpose of the conducted experiments was to initially estimate the values of accelerations acting especially on the passenger at selected driving speeds. On the basis of conducted tests, it was possible to verify the numerical model of the vehicle overcoming the obstacle on the road. This approach allows the use of the proposed model to verify the forces and accelerations affecting the passenger, specified before any selected specific biomechanical model of the human person, for example, a model of pregnant women in this configuration allows us to estimate the forces and accelerations acting on the embryo while overcoming some obstacles on the road.

1. INTRODUCTION

Speed bumps are safety devices designed to enforce the physical limitation of the speed of vehicles passing through them. Transverse obstacles, i.e., speed bumps and thresholds, can only be used on road sections where an effective speed limit is necessary – this may be the case where pedestrians have increased in a given area [12].

Thresholds can be divided on the basis of their shape, such as:

- island release bands

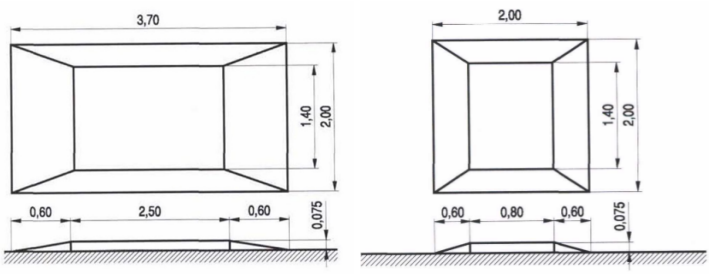

Fig. 1. Example of an island releasing threshold [12]

- Plate type and strip type

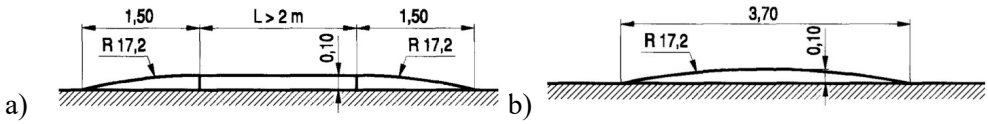

Fig. 2. Linear release threshold: a) plate with a limited speed of travel: 25-30km/h [1], b) slat with a limited speed of travel: 25-30km/h [12]

Each release threshold should be preceded by the occurrence of the A-11a sign with an indication of whether it occurs individually or in series. In the case of serial releases, determine the distances between them based on the occurring traffic situations, the speed of passing vehicles, etc. [9, 10, 12].

Fig. 3. Vertical marking of the serial release ramp, in which the distance between consecutive thresholds is not less than 20m and with a speed limit of 30km/h [12]

Thresholds are thresholds (Fig. 4) that apply outside of public roads. They are most often used at car park entrances, at entrances to company sites, on roads inside the dense housing and housing estates, and as a means of disciplining internal traffic [12].

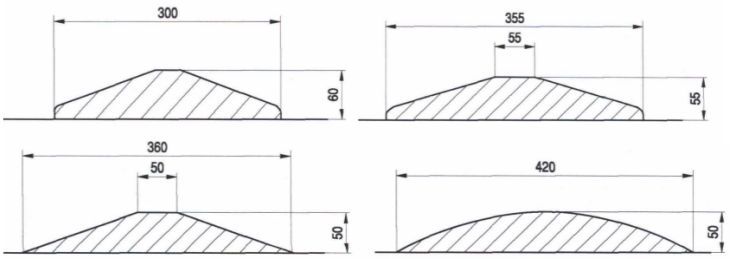

Fig. 4. Examples of the cross-section of typical throw thresholds [12]

Passenger cars are vehicles consisting of many harmonizing systems. The article focuses on the suspension of the vehicle. In passenger cars, it performs primarily the function of mitigating shocks, which arise in the results of passing over irregularities in the surface - in this case, on the thresholds of slowing down.

The article focuses on the construction of a phenomenological car suspension model with an accompanying biomechanical model of the human being giving the opportunity to study the interaction between the vibrating surface which is the threshold and the vehicle and the passenger and driver, respectively, with an emphasis on the passenger. As part of the research problem, a phenomenological model of the vehicle was developed along with the driver and passenger model. On the basis of the phenomenological model, a mathematical model was created, forming a formal basis

for the simulations in order to show the value of vertical vibration amplitudes affecting the body of the passenger and driver while passing through the speed bumps, where then these values were verified on the real object. The experiment consisted of triple crossing through the threshold in three series for speeds: 10km/h, 20km/h and 30km/h.

2. TEST OBJECT

In this article, a Skoda passenger car has been tested. In the vehicle, there was a driver and a passenger behind the driver's seat. The technical data of the test vehicle are summarized in Table 1.

Table 1

Technical data of the test vehicle

Technical data	Value	Unit
Mass of the vehicle	1095	[kg]
Wheelbase	2.462	[m]
Engine capacity	1.4	[l]
Maximum engine power	50	[kW]
Front Axle pressure	6.786	[kN]
Rear axle pressure	4.524	[kN]
Maximum speed	175	[km/h]

Fig. 5 shows the release threshold, which served as a horizontal obstacle during the test. This threshold is a threshold of type PZ-60/5.

Fig. 5. The threshold of type PZ-60/5

In Table 2, technical data of tested speed bump are presented. Particular attention should be paid to the height of the speed bump.

Table 2

Technical data of tested speed bump

Technical data	Value	Unit
Rollover length	64	[m]
Width	50	[m]
Height	5	[m]
Weight	14	[kg]
Mounting Holes	4	[-]

The speed bump is made of a rubber mixture. Each element is equipped with reflective elements. It consists of elements of the PZ-60/5 threshold and two ZPZ-60/5 ends. An appropriate element of vertical marking is shown in Fig. 3 [9, 10, 12].

3. PHENOMENOLOGICAL MODEL OF A RESEARCH OBJECT

One of the most popular dynamic models for vehicle suspensions is the half-model. The dynamic model presented in the article is a classic half-size model widely used in the literature [1, 3, 5, 6, 8, 15, 18, 22-24], in which the biomechanical model of the passenger and the driver in the form of a reduced mass along with the seat was also distinguished. For the purposes of modelling the seated passenger, a biomechanical model of the 6-DOF person sitting of Muksian and Nash was used [2, 13, 16].

In table 3, physical parameters describing the dynamic system are presented. The dynamic systems were divided into inertia elements, elastic elements, damping elements and other system parameters.

Table 3

Physical parameters describing the dynamic system

L.p.	Mark	Value	Dimension	L.p.	Mark	Value	Dimension
Inertia elements							
1	m_{1p}	22.23	kg	9	m_{1df}	40	kg
2	m_{2p}	5.921	kg	10	m_{1d}	58	kg
3	m_{3p}	0.455	kg	11	m_{1pf}	40	kg
4	m_{4p}	1.362	kg	12	m	1072.9	kg
5	m_{5p}	27.762	kg	13	m_1	13.6	kg
6	m_{6p}	6.82	kg	14	m_2	13.6	kg
7	m_{7p}	6.45	kg	15	J	801.65	kg/m
8	m_{1pf}	40	kg				
Elastic elements							
1	k_{2p}	877	N/m	7	k_{7p}	52600	N/m
2	k_{3p}	877	N/m	8	k_c	100000	N/m
3	k_{4p}	877	N/m	9	k2	165000	N/m
4	k_{5p}	877	N/m	10	k_{1f}	27194	N/m
5	k_{56p}	52600	N/m	11	k_{1r}	24741	N/m
6	k_{6p}	52600	N/m				
Damping elements							
1	b_{2p}	292	Ns/m	7	b_{6p}	3580	Ns/m
2	b_{3p}	292	Ns/m	8	b_{7p}	3580	Ns/m
3	b_{4p}	292	Ns/m	9	b_c	2000	Ns/m
4	b_{5p}	292	Ns/m	10	b_2	750	Ns/m
5	b_{56p}	3580	Ns/m	11	b_1	1309	Ns/m
Other system parameters							
1	L	2.465	m	4	L_3	0.1	m
2	L_1	0.985	m	5	L_4	1.005	m
3	L_2	1.477	m				

The presented model contains 12 degrees of freedom mainly described by variables such as vertical displacements of body q_1 and masses of unsprung q_3 and q_4, and vertical displacements of masses corresponding to the chair, and masses representing the human body specifying movements of individual body parts of the human biomechanical model. The model also includes the inclination of the body, represented by the angle φ. The parameter k_2 describes tire susceptibility at a pressure of 2.2 bar [14]. The physical parameters of the model are described in Table 3.

Forcing signal is the irregularity of the road in the form of a shifting threshold [17, 19] - semi-circular model, where other types of thresholds are also not excluded [11, 20, 21]. The equation that describes the obstacle being tested is given in formula 1. The value of the vertical displacement is in this case dependent on the vehicle speed and the height and width of the throw threshold. The following is a road profile which has been described by the function (eq. 1, 2, 3) as below [18, 19]:

$$\begin{cases} q_{10}=0.5A\left(1-\cos\left(\pi V_p L_p^{-1} t\right)\right) \\ q_{20}=0.5A\left(1-\cos\left(\pi V_p L_p^{-1}(t-\tau)\right)\right) \end{cases} \quad (1)$$

where t time, A - obstacle height, and τ - delay.

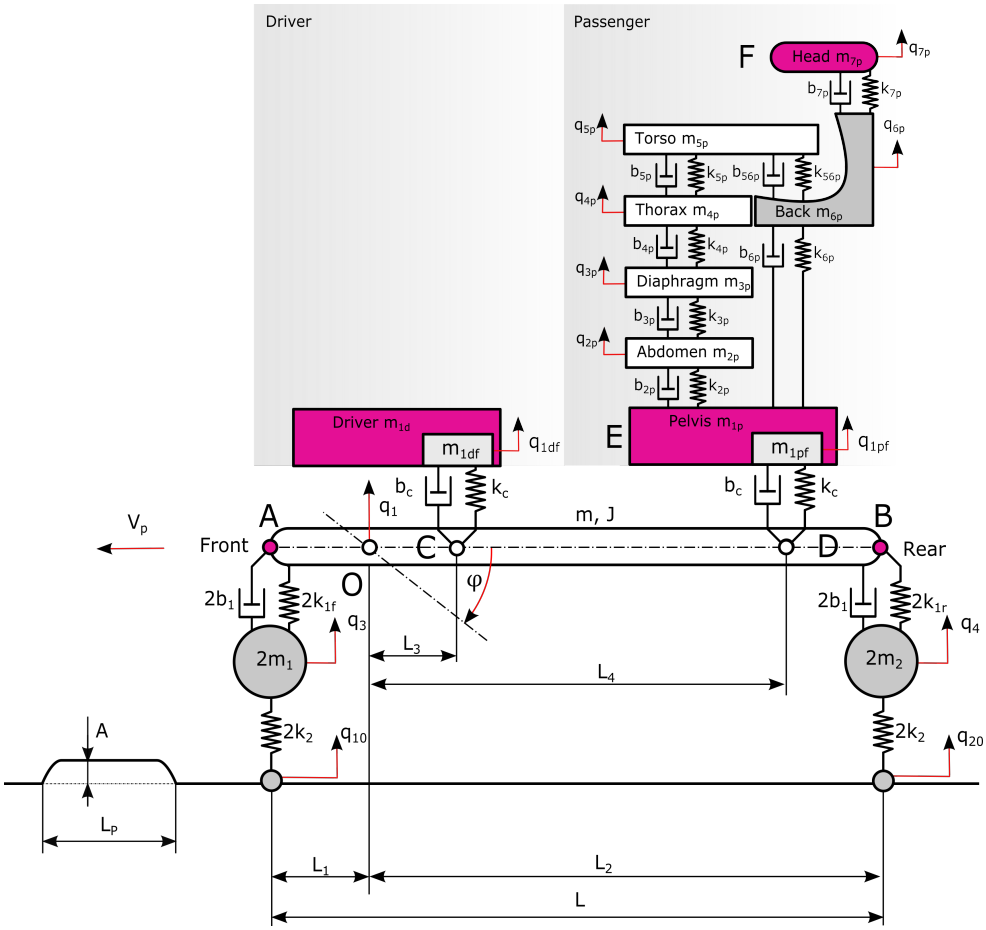

where A – obstacle height, L_p – obstacle length, V_p – vehicle speed, m – sprung mass, k_2 – tire stiffness, m_1 – unsprung weight on the front axle, m_2 – unsprung weight on the rear axle, J – moment of inertia of the sprung mass, k_{1f} and k_{1r} – suspension rigidity – front and rear, respectively, b_1 – damping shock absorber, k_c – rigidity of driver and passenger seat mounting, b_c – damping driver and passenger seat mounting, m_{1df} and m_{1pf} – seat weight, m_{1d} – driver weight, m_{2p}, m_{3p}, m_{4p}, m_{5p}, m_{6p}, and m_{7p} – masses of the biomechanical model of the passenger, and k_{3p}, k_{4p}, k_{5p}, k_{6p}, k_{7p} b_{3p}, b_{4p}, b_{5p}, b_{6p}, and b_{7p} – elastic-damping parameters of the passenger's biomechanical model.

Fig. 6. A phenomenological model of suspension with the driver and passenger

The delay was expressed as:

$$\tau = LV_p^{-1}. \quad (2)$$

Finally, the functions describing the forcing of vertical wheel displacement are described in the following relations:

$$q_{10}=\begin{cases} 0.5A\left(1-\cos\left(\pi V_p L_p^{-1} t\right)\right) & \text{, for } 0\le t\le\left(2L_p V_p^{-1}\right) \\ 0 & \text{, for } t>\left(2L_p V_p^{-1}\right) \end{cases} \quad (3)$$

$$q_{20}=\begin{cases}0.5A\left(1-\cos\left(\pi V_p L_p^{-1}(t-\tau)\right)\right) & \text{, for } 0\leq t\leq(2L_pV_p^{-1}+\tau)\\ 0 & \text{, for } t>\left(2L_pV_p^{-1}+\tau\right)\end{cases}.$$

The test involved a vehicle that tripled three times over the speed limit. Sample function sequences and sample runs of specific functions are shown in Fig. 7.

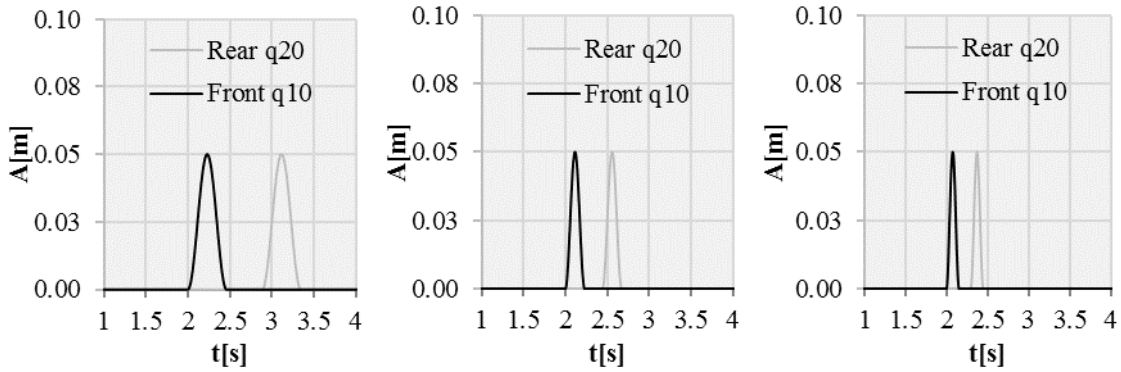

Fig. 7. Profiles forcing vertical vibrations while passing through the threshold for 10, 20, and 30 km/h, respectively

4. EQUATIONS OF MOTION

The model was based on the concept of generalized coordinates and the phenomenological model presented in Fig. 6. On their basis, the mass equations of the system were formulated using the method suggested by Lagrange [4]:

$$\frac{d}{dt}\left(\frac{\partial E_k}{\partial \dot{q}_j}\right)-\frac{\partial E_k}{\partial q_j}+\frac{\partial E_p}{\partial q_j}+\frac{\partial E_R}{\partial \dot{q}_j}=F_j, j=1,2,\ldots,n\ , \tag{4}$$

where t – time [s]; q_j – generalized displacement [m]; $\dot{q}_j$ – generalized speed [m/s]; n – number of degrees of freedom [-]; F_j – generalized force [N]; E_k – kinetic energy [J]; E_p – potential energy [J]; and E_R – dissipation function [J/s].

Based on the above equation and the model presented in Fig. 6, 12 dynamic motion equations were formulated:

$$\begin{cases}m_{2p}\ddot{q}_{2p}-k_{2p}(q_{1pf}-q_{2p})+k_{3p}(q_{2p}-q_{3p})-b_{2p}(\dot{q}_{1pf}-\dot{q}_{2p})+b_{3p}(\dot{q}_{2p}-\dot{q}_{3p})=0\\ m_{3p}\ddot{q}_{3p}-k_{3p}(q_{2p}-q_{3p})+k_{4p}(q_{3p}-q_{4p})-b_{3p}(\dot{q}_{2p}-\dot{q}_{3p})+b_{4p}(\dot{q}_{3p}-\dot{q}_{4p})=0\\ m_{4p}\ddot{q}_{4p}-k_{4p}(q_{3p}-q_{4p})+k_{5p}(q_{4p}-q_{5p})-b_{4p}(\dot{q}_{3p}-\dot{q}_{4p})+b_{5p}(\dot{q}_{4p}-\dot{q}_{5p})=0\\ m_{5p}\ddot{q}_{5p}-k_{5p}(q_{4p}-q_{5p})-k_{56p}(q_{6p}-q_{5p})-b_{5p}(\dot{q}_{4p}-\dot{q}_{5p})-b_{56p}(\dot{q}_{6p}-\dot{q}_{5p})=0\\ m_{6p}\ddot{q}_{6p}-k_{6p}(q_{1pf}-q_{6p})+k_{7p}(q_{6p}-q_{7p})+k_{56p}(q_{6p}-q_{5p})-\\ +b_{6p}(\dot{q}_{1pf}-\dot{q}_{6p})+b_{7p}(\dot{q}_{6p}-\dot{q}_{7p})+b_{56p}(\dot{q}_{6p}-\dot{q}_{5p})=0\\ m_{7p}\ddot{q}_{7p}-k_{7p}(q_{6p}-q_{7p})-b_{7p}(\dot{q}_{6p}-\dot{q}_{7p})=0\end{cases} \tag{5}$$

$$\begin{cases}(m_{1df}+m_{1d})\ddot{q}_{1df}=k_c(q_1-L_3\varphi-q_{1df})+b_c(\dot{q}_1-L_3\dot{\varphi}-\dot{q}_{1df})\\ (m_{1pf}+m_{1p})\ddot{q}_{1pf}+k_{2p}(q_{1pf}-q_{2p})+k_{6p}(q_{1pf}-q_{6p})+b_{2p}(\dot{q}_{1pf}-\dot{q}_{2p})+b_{6p}(\dot{q}_{1pf}-\dot{q}_{6p})=\\ =k_c(q_1-L_4\varphi-q_{1pf})+b_c(\dot{q}_1-L_4\dot{\varphi}-\dot{q}_{1pf})\end{cases} \tag{6}$$

$$\begin{cases}2m_1\ddot{q}_3=2k_2(q_{10}-q_3)-2k_{1f}(q_3-q_1-L_1\varphi)-2b_1(\dot{q}_3-\dot{q}_1-L_1\dot{\varphi})\\ 2m_2\ddot{q}_4=2k_2(q_{20}-q_4)-2k_{1r}(q_4-q_1-L_2\varphi)-2b_1(\dot{q}_4-\dot{q}_1-L_2\dot{\varphi})\end{cases} \tag{7}$$

$$\begin{cases} m\ddot{q}_1 - 2k_{1f}(q_3 - q_1 - L_1\varphi) - 2k_{1r}(q_4 - q_1 - L_2\varphi) + k_c(q_1 - L_3\varphi - q_{1df}) + k_c(q_1 - L_4\varphi - q_{1pf}) + \\ -2b_1(\dot{q}_3 - \dot{q}_1 - L_1\dot{\varphi}) - 2b_1(\dot{q}_4 - \dot{q}_1 - L_2\dot{\varphi}) + b_c(\dot{q}_1 - L_3\dot{\varphi} - \dot{q}_{1df}) + b_c(\dot{q}_1 - L_4\dot{\varphi} - \dot{q}_{1pf}) = 0 \\ J\ddot{\varphi} - L_1 2k_{1f}(q_3 - q_1 - L_1\varphi) - L_2 2k_{1r}(q_4 - q_1 - L_2\varphi) - L_3 k_c(q_1 - L_3\varphi - q_{1df}) - L_4 k_c(q_1 - L_4\varphi - q_{1pf}) + \\ -L_1 2b_1(\dot{q}_3 - \dot{q}_1 - L_1\dot{\varphi}) + L_2 2b_1(\dot{q}_4 - \dot{q}_1 - L_2\dot{\varphi}) - L_3 b_c(\dot{q}_1 - L_3\dot{\varphi} - \dot{q}_{1df}) - L_4 b_c(\dot{q}_1 - L_4\dot{\varphi} - \dot{q}_{1pf}) = 0 \end{cases} \quad .(8)$$

Based on the above-presented equations, a dynamic model of the tested object was constructed in the form of a Matlab/Simulink block diagram. Table 3 lists the physical parameters of the considered system.

5. RESULTS OF POLIGHIC AND SIMULATION TESTS

During the tests, the vehicle was equipped with 165/70 R14 series tires with a front pressure of 2.2 bar and a rear 2.2 bar. The road test was carried out for a standard set of the shock absorber. Fig. 8 shows the research vehicle along with the location of measurement nodes marked as A, A ', B, B', E, and F, where A and A ' – acceleration sensors located above the wheels of the front axle, B and B' – sensors located above the wheels rear axle, E – sensor located on the passenger's pelvis, and F - sensor located on the passenger's head.

The measurements were made using a set of experimental wireless acceleration sensors based on the MPU6050 system, with a 16-bit resolution and sampling frequency of 500 Hz for 2 measuring axes (Fig. 8) for points A, A', B and B' and a set of PhidgetSpatial Precision 0/0/3 High Resolution sensors, with a sampling rate of 250 Hz and 16-bit resolution. The data were saved using the Bluetooth interface on a laptop computer and the USB 2.0 interface for Phidget series devices.

Figs. 9, 10, and 11 summarize the time courses of the vertical acceleration values during the passage of the test vehicle successively through the threshold speeds of 10, 20 and 30 km/h for the rear axle, pelvis, and head of the passenger, respectively.

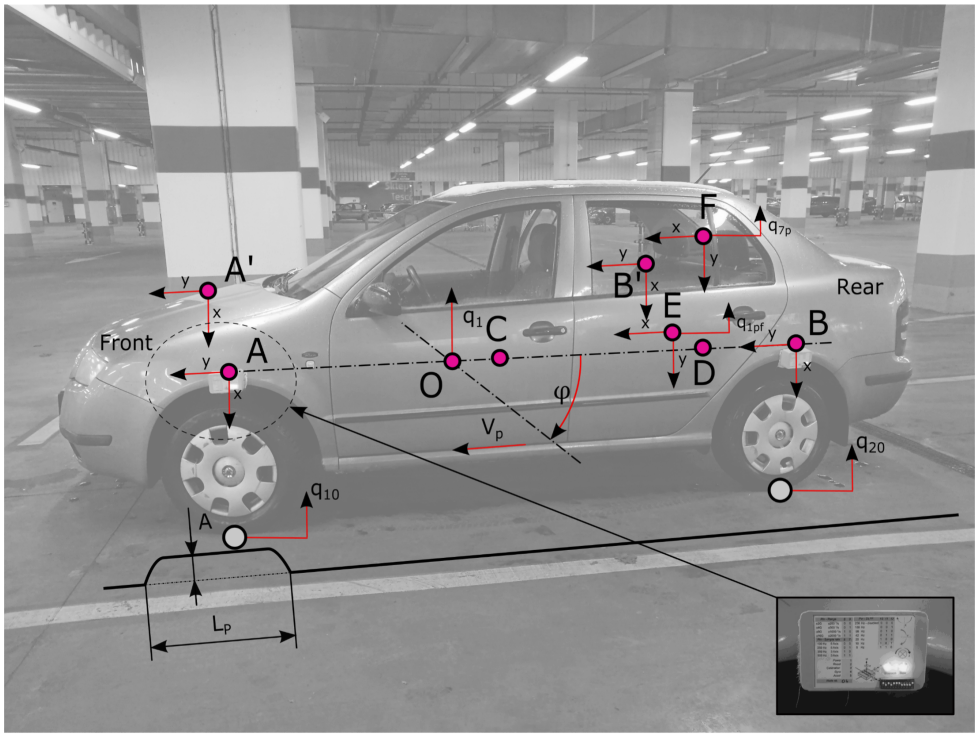

Fig. 8. A view of the research car and the measuring equipment mounted outside the car along with the presented forces

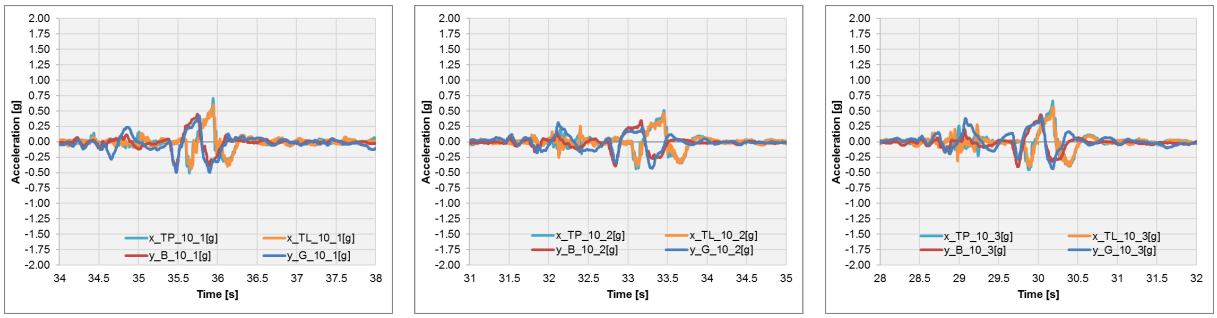

Fig. 9. Values of vertical accelerations during the passage through the speed threshold of 10 km/h for the next three tests, where x_TL – rear axle side after driver (Left), x_TP – rear axle passenger side (Right), y_B – vertical passenger pelvis movements, and y_G – vertical vibrations of the passenger's head

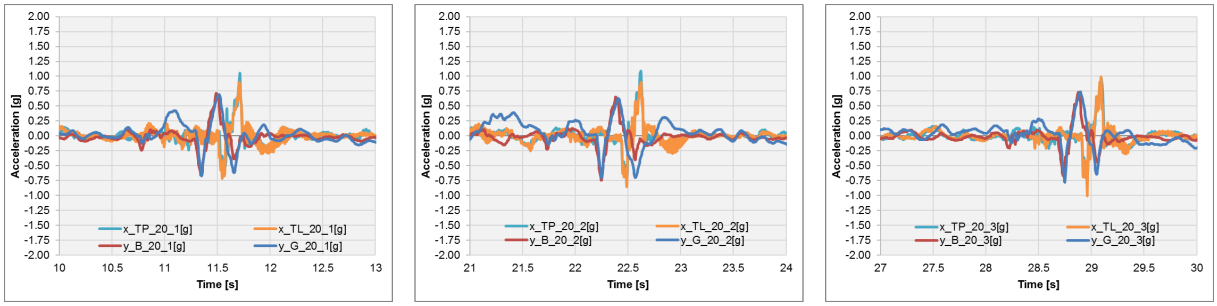

Fig. 10. Values of vertical accelerations during the passage through the speed threshold of 20 km/h for the next three tests, where x_TL – rear axle side after driver (Left), x_TP – rear axle passenger side (Right), y_B – vertical passenger pelvis movements, and y_G – vertical vibrations of the passenger's head

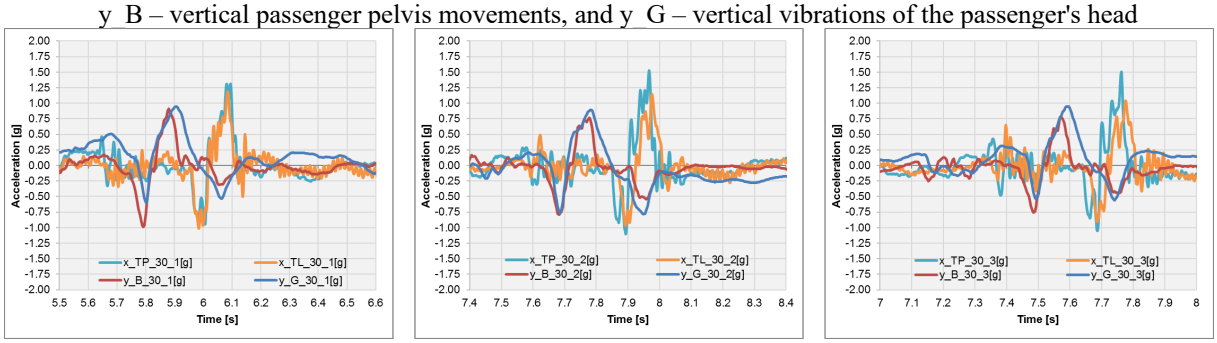

Fig. 11. The values of vertical accelerations during the trip through the speed threshold of 30 km/h for the next three tests, where x_TL – rear axle side after driver (Left), x_TP – rear axle passenger side (Right), y_B – vertical passenger pelvis movements, and y_G – vertical vibrations of the passenger's head

Figs. 12a, 12b, and 12c summarize the time courses of the vertical acceleration values during the passage of the test vehicle successively through the threshold speeds of 10, 20, and 30 km/h for the rear axle as well as the pelvis and head of the passenger, obtained by numerical simulation.

The following data were obtained on the basis of numerical simulation: for a speed of 10 km/h, the peak-to-peak force value of 2914 N and acceleration of 0.81 g affect the back of the vehicle, peak-to-peak force value of 848 N and acceleration of 0.75 g affect the pelvis, and peak-to-peak force value of 52 N and acceleration of 0.82 g affect the head.

For a speed of 20 km/h, peak-to-peak force value of 4702 N and acceleration of 1.47 g affect the back of the vehicle, peak-to-peak force value of 1291 N and acceleration of 1.37 g affect the pelvis, and peak-to-peak force value of 91 N and acceleration of 1.45 g affect the head. For a speed of 30 km/h, peak-to-peak force value of 6343 N and acceleration of 2.2 g affect the back of the vehicle, peak-to-peak force value of 1317 N and acceleration of 1.56 g affect the pelvis, and peak-to-peak force value of 98 N and acceleration of 1.55 g affect the head.

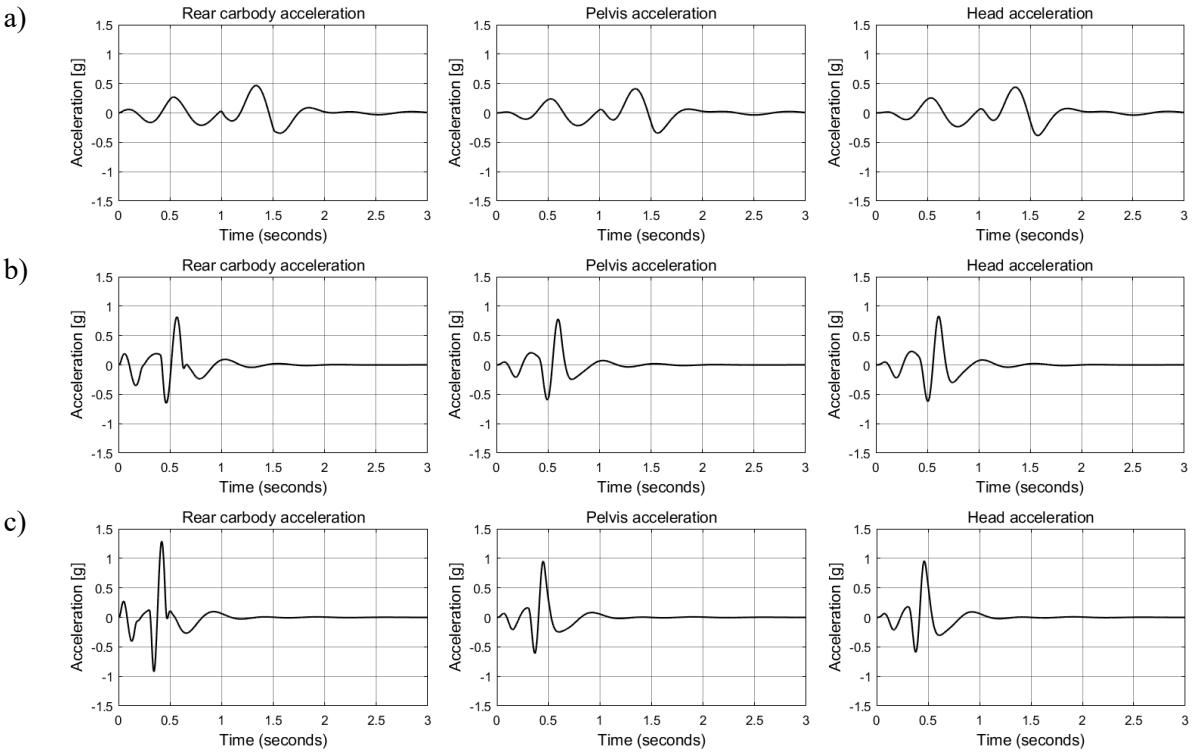

Fig. 12. Time series of accelerations affecting the back of the car and passenger during the passage through the threshold speed of a) 10 km/h, b) 20 km/h, and c) 30 km/h

The data obtained on the basis of tests and simulations are included in the list of values of vertical maximum accelerations during the passage through the threshold with selected speeds affecting the head, pelvis of the passenger, and rear of the vehicle, as shown in Fig. 13. As can be seen in Figs. 9-12, the higher the speed during the journey by the speed bump, the higher the acceleration values. When traveling at a speed of 30 km/h, the amplitude of the vertical acceleration for the rear axle reaches values in the range -0.92 g and 1.29 g, thus causing discomfort to the passenger, where the accelerations affecting the head are -0.59 g a 0.95 g; these accelerations are accompanied by forces corresponding, respectively, to a peak-to-peak value of 98 N for the head and 6343 N for the rear axle.

Fig. 13 compares the values obtained by simulation and research on the real object. As can be seen in Fig. 14, the maximum values of both negative and positive differences reach 22%. The differences result primarily from the adopted model simplifications, such as the linearization of suspension elements or the speed bump model.

The developed results show that a 30 km/h pass significantly influences the condition of the body, and it can also cause damage. In addition, traveling at this speed causes discomfort to passengers and it is already noticeably felt by both the driver and the passenger of the vehicle.

6. CONCLUSIONS

Speed bumps with a special distinction of ejection thresholds are devices increasingly used to limit the speed of vehicles. They are used primarily in places particularly frequented by both vehicles and pedestrians. As they are located in the vicinity of pedestrian crossings, the values of the forces that affect the human body when passing through a given threshold are significant in the parking lots in front of the shopping centers or in the housing estates. Due to the disciplining nature of the thresholds for drivers, aimed at reducing speed in these particularly dangerous places, drivers should be alerted by vertical signs.

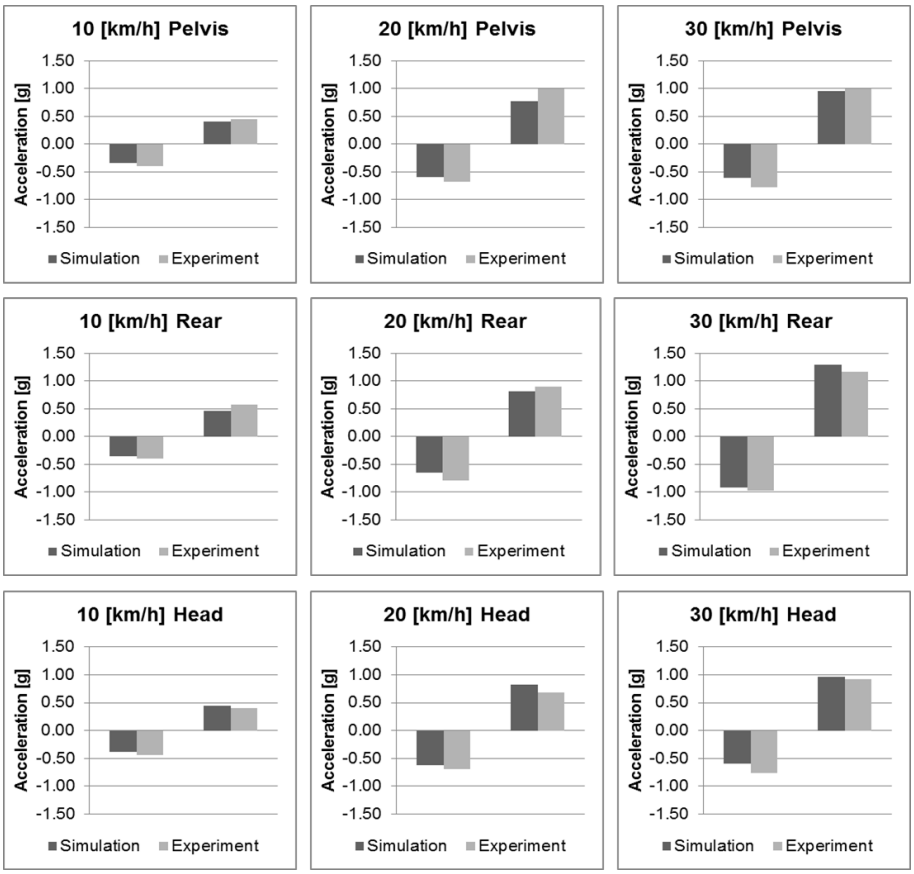

Fig. 13. The list of values of vertical maximum accelerations during the passage through the speed bump with the selected speeds affecting the head, pelvis of the passenger, and the rear of the vehicle

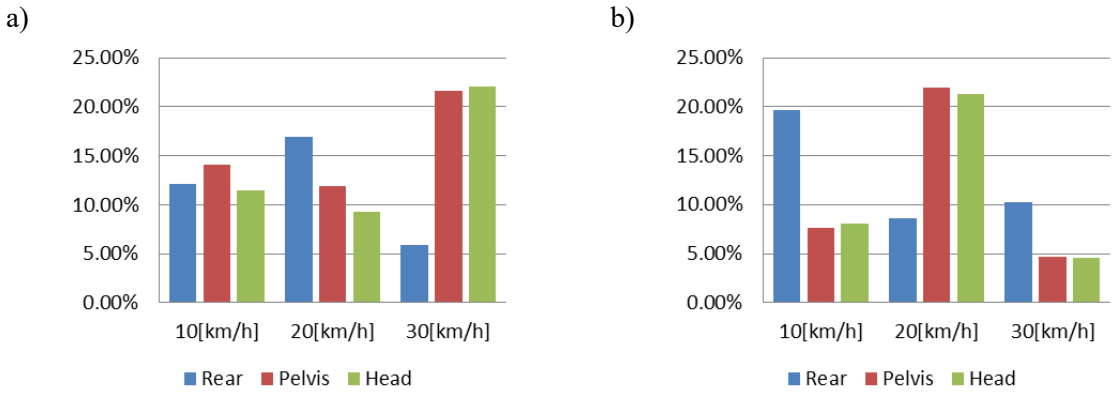

Fig. 14. Percentage differences of the measured values and data obtained by numerical simulation: a) for the maximum negative values and b) for the maximum positive values appropriate for the passenger's pelvis, head and the rear suspension

The tests carried out in this article were aimed at assessing the vertical accelerations and forces occurring in the vehicle during the passage through the speeding thresholds and the assessment of the impact of the release threshold on the passenger's body and comfort. The research shows that a passage complying with the law and limited speed up to 30 km/h may already be felt by people in the vehicle and the values of forces affecting the passenger's pelvis reach 804 N, where the peak-to-peak value is as much as 1317 N. An unexpected approach to the threshold at a speed of 30 km/h and often higher can cause sudden passenger recalls caused by a feeling of impact-related force. The approach

proposed in the article allows us to use the proposed model for the verification of forces and accelerations affecting the passenger, such as the pregnant woman model enabling in this configuration an estimation of forces acting and acceleration of the fetus during overcoming selected road obstacles. Considering the data obtained because of the conducted analyzes, it is beneficial to consider the use of other types of thresholds, such as sinusoidal thresholds having a much smaller impact on the vehicle and passenger due to its construction.

References

1. Abbas, W. & Emam, A. & Badran, S. & Shebl, M. & Abouelatta, O. Optimal Seat and Suspension Design for a Half-Car with Driver Model Using Genetic Algorithm. *Intelligent Control and Automation*. 2013. Vol. 4. No. 2. P. 199-205.
2. AlShabi, M. & Araydah, W. & ElShatarat, H. & Othman, M. & Younis M.B. & Gadsden, S.A. Effect of Mechanical Vibrations on Human Body. *World Journal of Mechanics*. 2016. Vol. 06(09). P. 273-304.
3. Badri, P. & Amini, A. & Sojoodi, M. Robust fixed-order dynamic output feedback controller design for nonlinear uncertain suspension system. *Mechanical Systems and Signal Processing.* 2016. Vol. 80. P. 137-51.
4. Cannon, R.H. *Dynamika układów fizycznych.* WNT. Warszawa, 1973. [In Polish: Dynamics of physical systems, WNT. Warszawa, 1973].
5. Choi, S.B. & Kim, W.K. Vibration control of a semi-active suspension featuring electrorheological fluid dampers. *Journal of Sound and Vibration*. 2000. Vol. 234. No. 3. P. 537-46.
6. Chróst, P. & Margielewicz, J. Modeling the vertical dynamics of a car on an mechatronic basis. *Scientific Journal of Silesian University of Technology. Series Transport*. 2015. Vol. 88. P. 19-29.
7. Hassaan, G.A. Car Dynamics using Quarter Model and Passive Suspension, Part I: Effect of Suspension Damping and Car Speed. *International Journal of Computer Techniques*. 2014. Vol. 1. No. 2. P. 1-9.
8. Huang, C.J. & Lin, J.S. & Chen, C.C. Road-adaptive algorithm design of half-car active suspension system. *Expert Systems with Applications*. 2010. Vol. 37. No. 6. P. 392-402.
9. Janczur, R. VBOX and V-SIM – from road tests of the car to computer simulation of its movement. In: *VIII International Conference Science-Technical, Safety problems in vehicles automotive"*. Kielce. 6-8 February 2012. P. 114-122.
10. Szczypiński-Sala W., Strzępek P., R. Janczur R. *Weryfikacyjne metody pomiaru opóźnienia hamowania pojazdu. Logistyka.* 2012. № 3. C. 2173-2177. [In Polish: *Comparative methods in the analyses of car brake deceleration. Logistics*. 2012. No. 3. P. 2173-2177]
11. Johnson, L. & Nedzesky, A. A comparative study of speed humps, speed slots and speed cushions. *Institution of Transportation Engineers.* 2004.
12. Dz.U. 2003 nr 220 poz. 2181. *Rozporządzenie Ministra Infrastruktury z dnia 3 lipca 2003 r. w sprawie szczegółowych warunków technicznych dla znaków i sygnałów drogowych oraz urządzeń bezpieczeństwa ruchu drogowego i warunków ich umieszczania na drogach*. [In Polish: Journal of Laws No. 220, item 211 and 2182. *Regulation of the Minister of Infrastructure of 3 July 2003. in the law of detailed technical conditions for road signs and signals as well as road safety devices and conditions for their placement on roads*.]
13. Liang, C.C. & Chiang, C.F. A study on biodynamic models of seated human subjects exposed to vertical vibration. *International Journal of Industrial Ergonomics*. 2006. Vol. 36. No. 10. P. 869-90.
14. Parczewski, K. Effect of tyre inflation preassure on the vehicle dynamics during braking manouvre. *Maintenance and Reliability*. 2013. Vol. 15. No. 2. P. 134-139.
15. Qassem, W. Model prediction of vibration effects on human subject seated on various cushions. *Medical Engineering & Physics*. 1996. Vol. 18. No. 5. P. 350-358.

16. Rakheja, S. & Dong R.G. & Patra, S & Boileau, P. & Marcotte, P. & Warren, C. Biodynamics of the human body under whole-body vibration: Synthesis of the reported data. *International Journal of Industrial Ergonomics.* 2010. Vol. 40. No. 6. P. 710-732.
17. Сладковский, А. & Погорелов, Д.Ю. Исследование динамического взаимодействия в контакте колесо-рельс при наличии ползунов на колесной паре. *Вісник Східноукраїнського національного університету.* 2008. No. 5(123) part 1. P. 88-95. ISSN 1998-7927. [In Russian: Sladkowski, A. & Pogorelov, D.Yu. Investigation of the dynamic interaction in the wheel-rail contact in the presence of flat spots on the wheelset. *Journal of East Ukrainian National University*].
18. Shirahatti, A. & Prasad, P.S.S. & Panzade, P. & Kulkarni, M.M. Optimal design of passenger car suspension for ride and road holding. *Journal of the Brazilian Society of Mechanical Sciences and Engineering*. 2008. Vol. 30. No. 1. P. 66-76.
19. Spinola Barbosa, R. Vehicle dynamic response due to pavement roughness. *Journal of the Brazilian Society of Mechanical Sciences and Engineering*. 2011. Vol. 33. No. 3. P. 302-307.
20. Weber, P. & Braaksma, J. Towards a North America geometric design standard for speed humps. *Institute of Transportation Engineering.* January, 2000. P. 30-34.
21. Mayer, S. & Viet, Le H. & Nesti, A. & Henze, N. The effect of road bumps on touch interaction in cars. *AutomotiveUI'18.* September, 23-25. Toronto. 2018.
22. Shelke, G.D. & Mitra, A.C. & Varude, V.R. Validation of Simulation and Analytical Model of Nonlinear Passive Vehicle Suspension System for Quarter Car. *Materials Today: Proceedings.* 2018. Vol. 5. No. 9. Part 3. P. 19294-19302.
23. Singh, D. Passenger body vibration control in active quarter car model using ANFIS based super twisting sliding mode controller. *Simulation Modelling Practice and Theory*. 2018. Vol. 89. P. 100-118.
24. Mohite, A.G. & Mitra, A.C. Development of Linear and Non-linear Vehicle Suspension Model. *Materials Today*: *Proceedings.* 2018. Vol. 5. No. 2. Part 1. P. 4317-4326.

Received 12.12.2017; accepted in revised form 05.03.2019